Journal of Sol-Gel Science and Technology (2024) 111:783–793
https://doi.org/10.1007/s10971-024-06489-4

ORIGINAL PAPER

Effect of fuel type and synthesis temperature on magnetic properties of $ZnFe_2O_4$ nanomaterials synthesized by sol-gel method

Ekaterina Bayan[1] · Maria Mokliak[1] · Yury Rusalev[2] · Mikhail Tolstunov[1,3]

Received: 28 May 2024 / Accepted: 11 July 2024 / Published online: 18 July 2024
© The Author(s), under exclusive licence to Springer Science+Business Media, LLC, part of Springer Nature 2024

Abstract

$ZnFe_2O_4$ nanomaterials were synthesized using the sol-gel method with different fuels: citric acid, tartaric acid, ascorbic acid and glucose monohydrate. The effects of organic fuel type and calcination temperature on the magnetic properties of zinc ferrite were studied. X-ray diffraction analysis, thermogravimetric analysis, differential scanning calorimetry, and transmission electron microscopy were used to investigate the process of zinc ferrite formation during the calcination of intermediate gel products, as well as to analyze the crystal structure and samples morphology. The formation of hematite and wurtzite secondary phases was confirmed for some materials, and the influence of heat treatment conditions on impurity formation was discussed. The particle size of zinc ferrite was 11–39 nm depending on the calcination temperature and selected fuel. According to data obtained using a vibrating sample magnetometer, the $ZnFe_2O_4$ nanoparticles exhibited ferrimagnetic behavior with saturation magnetization values of 1.92–15.61 emu/g. Changing the fuel type and the calcination temperature makes it possible to obtain $ZnFe_2O_4$ nanomaterials with specific magnetic properties.

Graphical Abstract

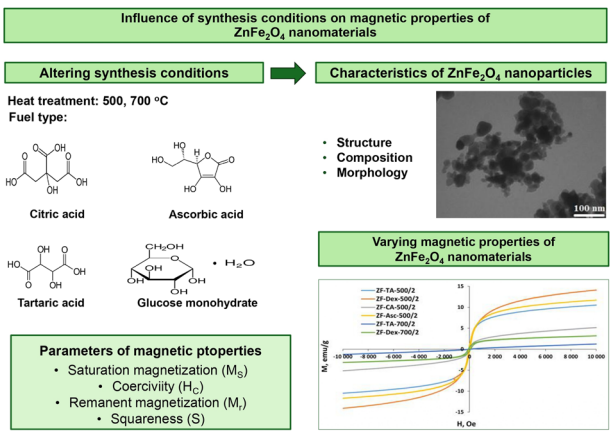

Keywords $ZnFe_2O_4$ · Ferrites · Sol-gel method · Fuel type · Magnetic properties

✉ Ekaterina Bayan
ekbayan@sfedu.ru

[1] Chemical Faculty, Southern Federal University, Rostov-on-Don, Russia

[2] The Smart Materials Research Institute, Southern Federal University, Rostov-on-Don, Russia

[3] Southern Scientific Center of Russian Academy of Science, Rostov-on-Don, Russia

Highlight

- Nanosized $ZnFe_2O_4$ samples were obtained by the sol-gel method using four fuels.
- The formation of zinc ferrite nanoparticles has been experimentally confirmed
- The effect of fuel on phase composition of $ZnFe_2O_4$ was studied by X-ray diffraction
- Zinc ferrite nanomaterials exhibit ferrimagnetic behavior at room temperature

1 Introduction

Nanosized magnetic material technology is still under development and has attracted the attention of researchers. Magnetic materials are currently used in electronics, information storage, biomedical applications, and environmental conservation [1–3]. The potential applications of these materials are determined by various factors, such as stability and safety for human health and the environment [4, 5], low cost, etc. Nanoscaled spinel ferrites are corresponding to these requirements. Nanosized ferrites with spinel structure are characterized be general formula MFe_2O_4 and are widely known as data recorders, energy storage devices [6], contrast agents for magnetic resonance imaging [7], sensors [8, 9], catalysts [10], heavy metal adsorbents [11, 12]. Zinc ferrite is a promising material, with a wide range of functional properties, including magnetic ones.

Zinc ferrite has a normal spinel type structure, in which Zn^{2+} ions occupy tetrahedral (A) positions, Fe^{3+} ions arranged in octahedral (B) lattice interstices. Such distribution of cations on sublattices is characteristic for bulk $ZnFe_2O_4$, which is antiferromagnetic at temperatures below $T_N = 9$ K, in contrast to nanoscale zinc ferrite, which exhibits ferrimagnetic or paramagnetic properties due to differences in the cation distribution between sublattices [13]. The magnetic properties of materials based on zinc ferrite are also influenced by the synthesis method and particle size [14], which is expressed in the dependence of saturation magnetization and coercivity on these parameters.

The most significant parameters for magnetic properties assessment of zinc ferrite materials are saturation magnetization (M_S) and coercivity (H_C). The range of optimal values for each parameter varies on the potential applications of $ZnFe_2O_4$ [15, 16]. The fabrication of zinc ferrite nanomaterials with easily tunable M_S and H_C is one of the high priority issues for researchers, which is solved by selecting the optimal synthesis method and controlling the processing conditions of the intermediate product [17, 18]. $ZnFe_2O_4$ is commonly prepared by co-precipitation [19], thermal decomposition [20], hydrothermal [21], and sol-gel processes [14, 22] and other methods. These methods provide the synthesis of zinc ferrite with different morphology, particle size and readily adjustable magnetic characteristics. All synthesis methods have both advantages and disadvantages: expensive equipment, duration of synthesis, low yield, etc. The advantages of using sol-gel method are simplicity and availability, relatively low energy consumption, obtaining homogeneous and chemically pure ferrite particles [23]. The most promising is the group of sol-gel methods using organic compounds that also act as fuels, such as urea [24], citric acid [25], glycine [26], starch [27], ethylene glycol [28], egg white [29]. The organic reagents used in the method strongly influence the operating temperature [7], combustion rate, which ultimately determines the morphology, composition, and structure of ferrite. Slatineanu et al. prepared zinc ferrite by an optimized sol-gel auto-combustion technique using six different precursors as fuels [30]. $ZnFe_2O_4$ nanoparticles were obtained by coprecipitation using surfactants from plants such as lemon, red pepper, black pepper, saffron, as well as gelatin, polyvinylpyrrolidone, and glucose. It was shown that the introduced additives influenced the morphology and size of $ZnFe_2O_4$ nanoparticles [31]. The measured magnetic properties for $ZnFe_2O_4$ samples indicated that ferrimagnetic nanomaterials can be obtained using glucose and glycine, while replacing the fuel with egg white leads to a change in the magnetism to paramagnetic behavior. A. Shanmugavani et al. performed a comparative analysis of the magnetic and electrical properties of zinc ferrite produced by combustion synthesized at different pH values using asparagic acid and glycine [32]. The results of the measurements revealed the paramagnetic nature of the materials with negligible coercivity and saturation magnetization less than 3.4 emu/g, depending more on the conductivity of the materials themselves than the fuel choice. R. C. Sripriya et al. synthesized zinc ferrite using glycine as fuel and two different heat treatment approaches: microwave irradiation and conventional one utilizing an air furnace [33]. The structural, magnetic and other materials properties were found to be influenced by the calcination temperature and the synthesis method. It is notable that heating the reaction mixture in a microwave oven led to an increase in the saturation magnetization of $ZnFe_2O_4$ compared to another sample calcined in the furnace. A. Kannolli et al. studied the effect of the calcination temperature of $ZnFe_2O_4$ prepared with citric acid on the morphology, structural and magnetic properties of the materials [34]. The analysis of the obtained results revealed that crystallite size and magnetization rise monotonically with increasing temperature from 350 to 550 °C. It is concluded from the literature data that to obtain zinc ferrite with favorable magnetic properties, combined effect of precursors and material heat treatment conditions should be studied.

The use of various fuels in the synthesis process makes it possible to obtain zinc ferrite powder materials that differ in magnetic properties. The properties of zinc ferrite powders change due to the dependence of saturation magnetization and coercivity on the structure, morphology, and phase composition of materials and particle size of ferrite [35]. These characteristics of zinc ferrite are related to the stability of complex compounds formed as a result of the organic fuels addition [36]. As we know, no previous research has investigated the use of ascorbic acid as a fuel for synthesizing zinc ferrite from inorganic iron and zinc salts by the sol-gel method. Therefore, in this work, the effect of this particular type of fuel was studied in comparison with other organic substances as a rule used as fuels, such as citric, tartaric acids and glucose monohydrate and capable of forming complexes with zinc and iron cations with different stability constants. In this work, we focused on studying the influence of widely available and low-cost fuels and calcination temperature on the phase composition, morphology, and magnetic properties of $ZnFe_2O_4$ nanomaterials obtained by sol-gel method. The magnetic characteristics of zinc ferrite synthesized using ascorbic acid have also been established for the first time.

2 Materials and methods

2.1 Materials and reagents

The precursors used for preparation of $ZnFe_2O_4$ were iron (III) nitrate nonahydrate $Fe(NO_3)_3{\cdot}9H_2O$ (JSC REACHIM LLC, Moscow, Russia), zinc nitrate hexahydrate $Zn(NO_3)_2{\cdot}6H_2O$ (NPP Aquatest LLC Rostov-on-Don, Russia), citric acid $C_6H_8O_7$ (NPP Aquatest LLC Rostov-on-Don, Russia), ascorbic acid $C_6H_8O_6$ (NPP Aquatest LLC Rostov-on-Don, Russia), tartaric acid $C_4H_6O_6$ (JSC REACHIM LLC, Moscow, Russia) and glucose monohydrate $C_6H_{12}O_6{\cdot}H_2O$ (NPP Aquatest LLC Rostov-on-Don, Russia). All precursors were of chemically pure grade analytical grade.

2.2 Synthesis of $ZnFe_2O_4$

A mixture of iron (III) nitrate and zinc (II) nitrate was dissolved in distilled water. To the obtained nitrate solution was added organic fuel (citric acid, tartaric acid, ascorbic acid or glucose monohydrate) considering the molar ratio: Zn:Fe:-Fuel = 1:2:3, stirred to homogeneous condition. The reaction mixture was evaporated at 100 °C with constant stirring until a gel was formed. The obtained gel was calcined in a muffle furnace in air atmosphere at 500 and 700 °C for 2 and 4 h. Heating was carried out at a rate of 10 deg·min^{-1}. The synthesized samples were named according to the heat treatment conditions and the fuel applied (Table 1).

Table 1 Synthesis parameters for the preparation of zinc ferrite materials

Sample name	Fuel	Thermal treatment conditions
ZF–CA–500/2	Citric acid	500 °C, 2 h
ZF–TA–500/2	Tartaric acid	
ZF–Asc–500/2	Ascorbic acid	
ZF–Dex–500/2	Glucose monohydrate	
ZF–CA–500/4	Citric acid	500 °C, 4 h
ZF–TA–500/4	Tartaric acid	
ZF–Asc–500/4	Ascorbic acid	
ZF–Dex–500/4	Glucose monohydrate	
ZF–CA–700/2	Citric acid	700 °C, 2 h
ZF–TA–700/2	Tartaric acid	
ZF–Asc–700/2	Ascorbic acid	
ZF–Dex–700/2	Glucose monohydrate	
ZF–CA–700/4	Citric acid	700 °C, 4 h
ZF–TA–700/4	Tartaric acid	
ZF–Asc–700/4	Ascorbic acid	
ZF–Dex–700/4	Glucose monohydrate	

2.3 Characterization of $ZnFe_2O_4$ materials

The phase composition of the obtained materials was studied by X-ray diffraction analysis (XRD) using the ARL X'TRA diffractometer. CuKα radiation was employed with the generator settings 40 kV and 30 mA. The XRD patterns were recorded in the range of Bragg angles $20° \le 2\Theta \le 80°$. The calculation of the coherent scattering regions was performed using the Scherrer equation (Formula 1):

$$D = \frac{k\lambda}{\beta \cos \Theta}, \quad (1)$$

where k is the shape factor, $\lambda = 0.1540562$ nm is the X-ray wavelength, β is the full width at the half maximum of the diffraction line and Θ is the diffraction angle.

Also, to assess the effect of microdeformations of the lattice, the crystallite sizes and lattice strain ε using the Williamson−Hall method was investigated [37].

The lattice constant (a) values of $ZnFe_2O_4$ for the obtained materials were determined by the following formula (Formula 2):

$$a = d\sqrt{h^2 + k^2 + l^2}, \quad (2)$$

where d is the interplanar spacing and h, k, l are Miller indices of diffraction planes.

The cell volume (V) was derived from the value of lattice constant a as shown in Formula 3:

$$V = a^3, \quad (3)$$

The X-ray density ρ_x of the synthesized nanoparticles have been determined using Formula 4:

$$\rho_x = \frac{8M}{N_A \cdot a^3}, \quad (4)$$

where M is molecular weight, N_A is Avogadro's number.

Thermogravimetric analysis (TGA) and differential scanning calorimetry (DSC) of gel intermediate products (ZF–TA–Gel, ZF–CA–Gel, ZF-Asc–Gel, ZF–Dex-Gel) were carried out using the NETZSCH STA 449 F3 Jupiter synchronous thermal analysis device under air atmosphere. The morphology of the samples was evaluated using transmission electron microscopy (TEM), a transmission electron microscope Tecnai G2 Spirit Bio TWIN operating at 120 kV. Magnetic properties of the zinc ferrite samples were measured using a vibrating sample magnetometer Lake Shore Model 7404, at room temperature. The parameter S (squareness) was calculated using Formula 5 [25]:

$$S = \frac{M_r}{M_S}, \quad (5)$$

where M_r is remanent magnetization, M_S is saturation magnetization.

3 Results and discussion

3.1 DSC and TGA studies of intermediate products

Figure 1 shows the results of TGA and DSC of gel intermediate products. Comparing the obtained data, it was revealed that thermal decomposition of gels is a multistage process, which can be divided into 4–5 segments. When heated to 100–120 °C, evaporation of moisture adsorbed from the environment occurs, accompanied by mass loss and endothermic effect. Up to 200 °C it is also possible to identify areas on TGA-curves, where a decrease in mass is observed due to the removal of chemically bound water. Further heating of samples at T = 200–300 °C leads to decomposition of the organic component in the reaction mixture, formation of oxide phases, which is confirmed by the data of TGA- and DSC-curves. Subsequent temperature increase contributes to the higher completeness degree of the organic component decomposition, phase transitions of inorganic compounds are possible accompanied by the formation of zinc ferrite. The final stage of the process is described by mass stabilization, absence of significant thermal effects.

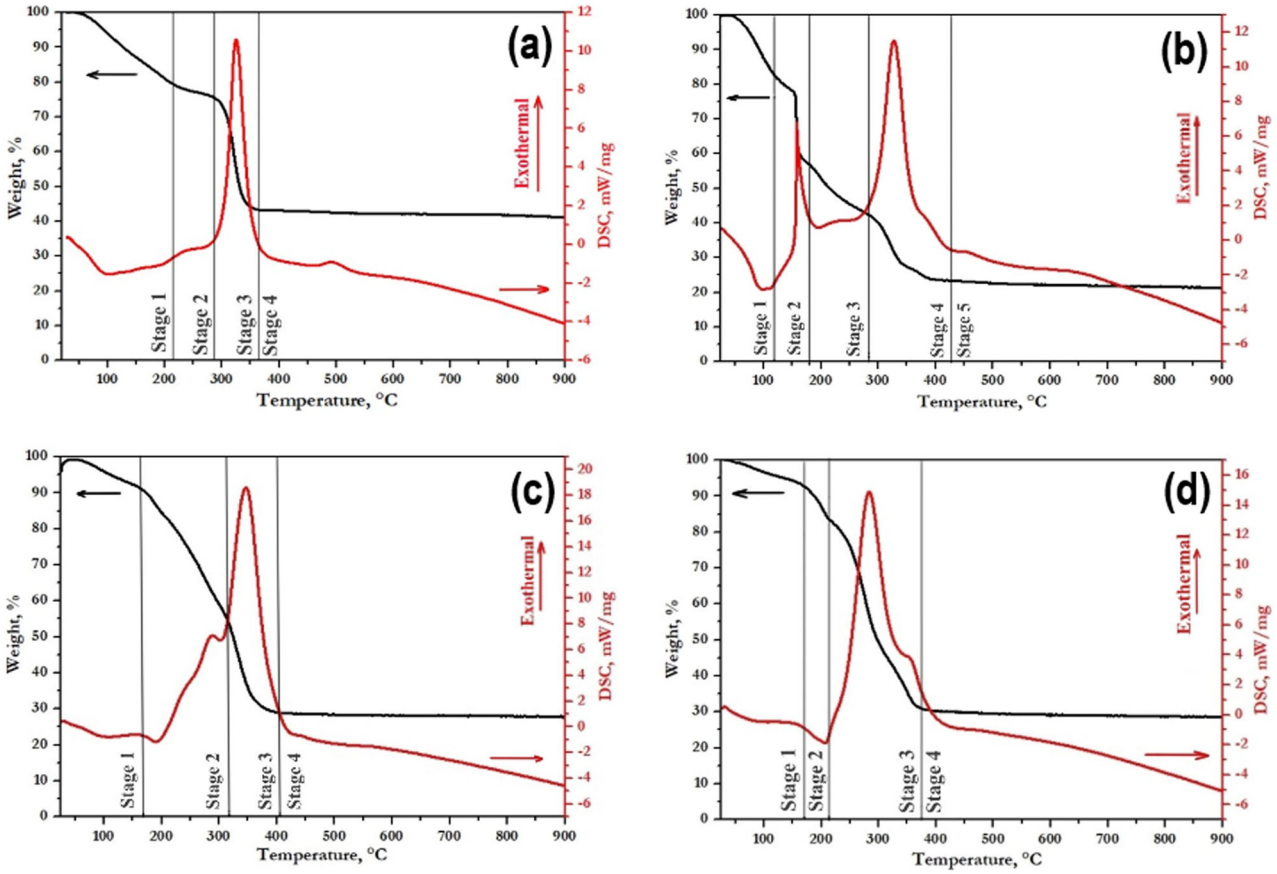

Fig. 1 TGA-DSC curves for (**a**) ZF–TA–Gel, (**b**) ZF–CA–Gel, (**c**) ZF–Dex–Gel, (**d**) ZF–Asc–Gel

According to the results of TGA and DSC of ZF-TA-Gel, the thermal decomposition of the gel can be divided into 4 stages with the corresponding regions marked in Fig. 1a. At stage 1 the temperature gradually increases up to 215 °C and the sample mass decreases by 20.6% due to the removal of absorbed moisture and bound water. In the temperature range from 215 to 288 °C, representing stage 2, the mass loss was 4.2% due to partial destruction of the tartrate complex. Further heating in the range of 288–365 °C leads to the complete removal of the organic phase, accompanied by the formation of oxide phases. At temperatures above 365 °C, no mass loss occurs, and no heat release or absorption is also observed.

Figure 1b shows the results of TGA and DSC of ZF-CA-Gel. The thermal decomposition process of this gel intermediate also occurs sequentially and is divided into 5 stages. Stage 1, representing the changes in the system at the initial moment at a temperature less than 118 °C, is characterized by a mass loss of 17.4% due to the evaporation of absorbed water. In stage 2, in the temperature range 118–180 °C, a mass loss of 25.9% is observed due to the removal of bound water from the gel. At 180–284 °C the organic components of the system decompose with the formation of intermediate oxide phases; the mass loss reaches 14.7%. As the temperature increases, the proportion of oxides in the reaction mixture gradually declines due to the formation of ferrite. The process of $ZnFe_2O_4$ final production occurs at stage 4, at a temperature of 284–429 °C and is also associated with the final removal of the organic phase, mass reduction by 19.1%. At higher temperatures at stage 5 no changes in the TGA curve are observed, indicating the completion of thermal decomposition.

TGA/DSC curves (Fig. 1c) are divided into 4 regions according to the stages of thermal decomposition of ZF-Dex-Gel. In stage 1 the temperature does not be greater than 169 °C and the mass loss is 9.4% due to the removal of absorbed and chemically bound water. There is a consecutive decomposition of the organic components of the system, intermediate oxide phases are formed at heating in the range of 169–405 °C. Furthermore, at stages 2 and 3 the formation of zinc ferrite phase occurs, accompanied by exothermic effect. During the decomposition of the reaction mixture components, the mass decreases by 36.7% at 169–317 °C and by 25.7% at 317–405 °C. At the last stage in the temperature range of 405–900 °C the mass is stable.

Figure 1d, divided into 4 fragments, shows the TGA and DSC data of ZF-Asc-Gel. In stage 1, at a temperature less than 170 °C, the weight change is 7.5%, which is attributed to the removal of bound and absorbed water from the gel. Further at the temperature of 170–214 °C the weight loss increases up to 9.4%, which is due to the beginning of decomposition of the organic component of the reaction mixture. The greatest weight loss, which is equal to 53.1%, occurs at the temperature of 214–376 °C. At this stage oxide phases are formed, and zinc ferrite formation is possible during the interaction. At the last stage at T = 376–900 °C the weight change and significant thermal effects are not evident. Thus, based on the DSC-TGA analysis, synthesis temperatures of 500 and 700 °C were selected. At lower temperatures, the spinel phase is just forming, and a large amount of impurities is also formed.

3.2 Effect of fuel type and synthesis temperature on phase composition and particle size of $ZnFe_2O_4$ materials

According to XRD data, the synthesized materials have a cubic structure typical for zinc ferrite (Fig. 2). Wurtzite and hematite phases were identified for some samples. The presence of secondary phases in the system is due to the formation of zinc and iron hydroxides as the side products during the synthesis of materials [34, 38]. At thermal decomposition of the corresponding hydroxides ZnO and α-Fe_2O_3 are formed, which is confirmed by XRD data of the materials. At the calcination temperature of 500 °C for samples ZF–CA–500/2, ZF-TA–500/2, aside from zinc ferrite, no secondary phases in the amorphous state were identified. The increase of the annealing temperature from 500 to 700 °C (duration of thermal treatment equals 2 h) contributes to the reduction of the amorphous component of the system, hematite and wurtzite phases are observed.

An increase in crystallinity of all materials was observed with prolongation of heat treatment time (Fig. 2c, d). For the samples synthesized at annealing temperatures of 500, 700 °C and 4 h of calcination in addition to the $ZnFe_2O_4$ phase, oxide impurities were also identified. The content of secondary phases diminishes with increasing temperature from 500 to 700 °C. It should be noted that the crystallite size of zinc ferrite increases both at longer calcination and at higher temperature.

According to the results of calculations, the values of the lattice constant a vary within 8.40–8.43 Å and remain close to the value of bulk material. It was found that particle size increases due to lower surface tension for some samples synthesized using citric and tartaric acids [39]. Deviations from the direct dependence of the lattice constant on particle size for materials obtained using ascorbic acid and glucose monohydrate can be associated with changes in the cation distribution over sublattices [40].

The formation of a considerable amount of secondary phases is specific for zinc ferrite synthesized using ascorbic acid and glucose monohydrate. This tendency is attributed to the low gel self-combustion temperature [30] and the different complexing ability of the initial organic substances. Citric, tartaric, ascorbic acids and glucose monohydrate during synthesis bind zinc and iron cations forming the metal complexes. Obtaining stable complexes prevents

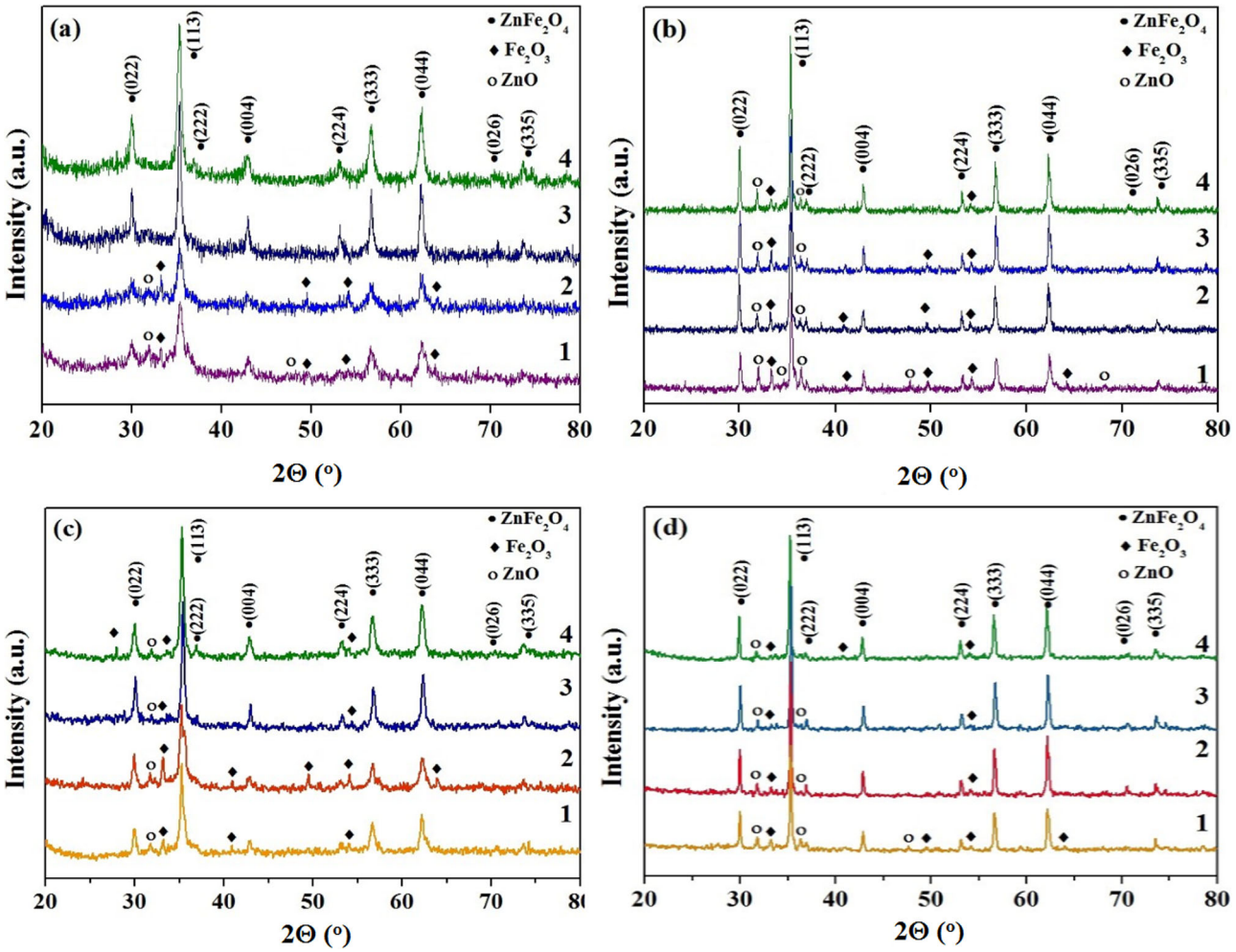

Fig. 2 XRD patterns of zinc ferrite materials obtained by the application of glucose monohydrate (1), ascorbic acid (2), tartaric acid (3), citric acid (4) as fuel, calcined at (**a**) 500 or (**b**) 700 °C for 2 h, (**c**) 500 or (**d**) 700 °C for 4 h. ZF – franklinite calculated from the crystallographic data [57]

the precipitation of zinc and iron hydroxides. In this case, the complexation reaction proceeds with a different degree of completion depending on the chelating agent. The stability constants of the formed citrate compounds vary from 10^5 ($ZnCit^{2-}$) to 10^{11} ($FeCit^{-}$) [41], while the tartrate ones are 10^3–10^5 for complex compounds with Zn and 10^7–10^{11} for complex compounds with Fe(III) [41], ascorbic acid and glucose are weak complexing agents, which is confirmed in previously published works [42, 43].

According to the XRD analysis results, the average crystallite size of the spinel phase was calculated using the Scherrer equation. The results of calculations are presented in Table 2. The lowest crystallite size was 11 nm for samples ZF–Asc–500/2 and ZF–Dex–500/2, the largest was 39 nm for ZF–Asc–700/4. It is also notable that elevating the gel calcination temperature leads to both increase in the crystallinity and the crystallite size.

Based on XRD data, we found that zinc ferrite powder materials calcined at 500 °C for 2 h (ZF-CA/500-2 and ZF-TA-500/2) were single-phase and crystallized in the spinel phase. These materials also had a smaller particle size compared to those calcined at either 700 °C or 4 h at 500 °C. As a result, $ZnFe_2O_4$ nanomaterials calcined at 500 °C were further investigated in more detail. The crystallite sizes of ZF–CA–500/2, ZF–TA-500/2, ZF–Asc-500/2, and ZF–Dex-500/2 nanoparticles were calculated by the Williamson-Hall method and were found to be 17, 24, 12, and 11 nm, respectively. In addition, the lattice strain values were obtained for ZF–CA–500/2, ZF–TA-500/2, ZF–Asc-500/2, ZF–Dex-500/2, which were 0.0008, 0.0011, 0.0012 and 0.0011, respectively.

As shown by TEM, the materials ZF–CA–500/2 and ZF–TA–500/2 synthesized by sol-gel method using citric and tartaric acids contain nanoparticles (Fig. 3). The particles are characterized by the occurrence of agglomerates forming conglomerates of several hundred nanometers in size. The heterogeneous arrangement of nanoparticles as well as the proximity of relatively lesser and greater

Table 2 Variation of crystallite size and lattice parameter of $ZnFe_2O_4$ nanomaterials

Sample name	Crystallite size, nm	Lattice constant a, Å	Cell volume, V ($Å^3$)	X-ray density, ρ_x (g/cm^3)
ZF–CA–500/2	15	8.42	596.48	5.37
ZF–TA–500/2	22	8.42	596.50	5.37
ZF–Asc–500/2	11	8.41	595.76	5.38
ZF–Dex–500/2	11	8.41	595.76	5.38
ZF–CA–500/4	17	8.42	597.31	5.36
ZF–TA–500/4	24	8.40	593.70	5.40
ZF–Asc–500/4	26	8.42	597.99	5.36
ZF–Dex–500/4	25	8.42	597.93	5.36
ZF–CA–700/2	34	8.42	596.84	5.37
ZF–TA–700/2	34	8.43	598.27	5.35
ZF–Asc–700/2	37	8.41	595.42	5.38
ZF–Dex–700/2	33	8.41	594.21	5.39
ZF–CA–700/4	36	8.43	598.80	5.35
ZF–TA–700/4	35	8.41	594.15	5.39
ZF–Asc–700/4	39	8.42	596.14	5.37
ZF–Dex–700/4	37	8.42	595.91	5.38

aggregates can be explained by the magnetic nature of nanoscale zinc ferrite [44, 45]. The average size of individual particles is about 14–19 and 21–26 nm for ZF–CA–500/2 and ZF–TA–500/2, respectively. The average crystallite size determined by TEM is close to crystallite size obtained from XRD data.

3.3 Effect of fuel type and synthesis temperature on magnetic properties of $ZnFe_2O_4$ materials

Figure 4 shows the magnetic hysteresis curves of the synthesized materials measured at room temperature. The values of saturation magnetization (M_S), remanent magnetization (M_r) and coercivity (H_C) were determined from the hysteresis loops. The measurement results for samples calcined at 500 °C for 2 h are shown in Table 3.

According to the obtained data, all samples are characterized by a narrow hysteresis loop, which is a particular feature of the soft magnetic materials [46, 47]. The materials magnetic properties were affected by the chosen

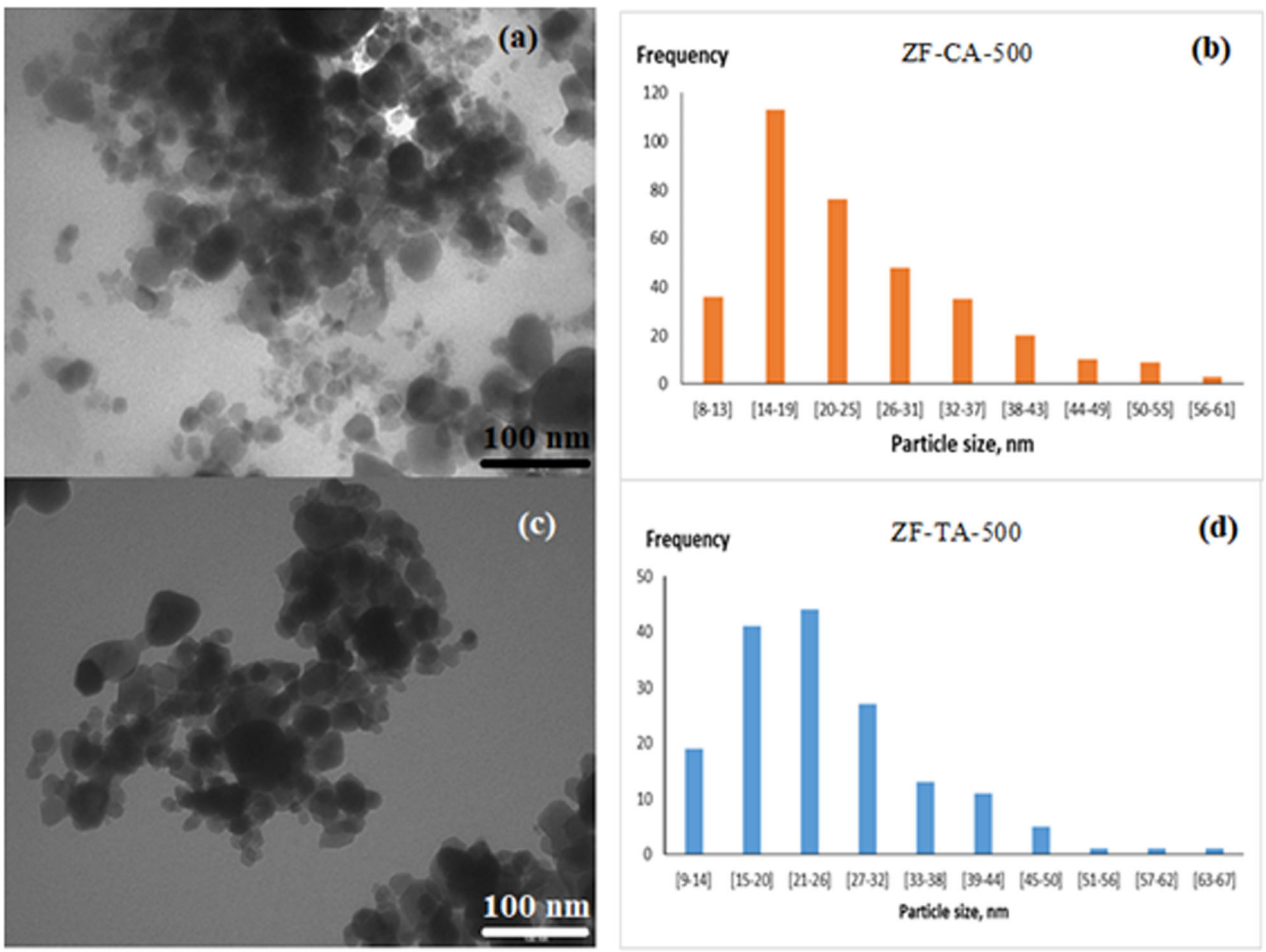

Fig. 3 TEM images and corresponding particle size distributions for $ZnFe_2O_4$ materials: (**a**, **b**) ZF–CA–500/2; (**c**, **d**) ZF–TA–500/2

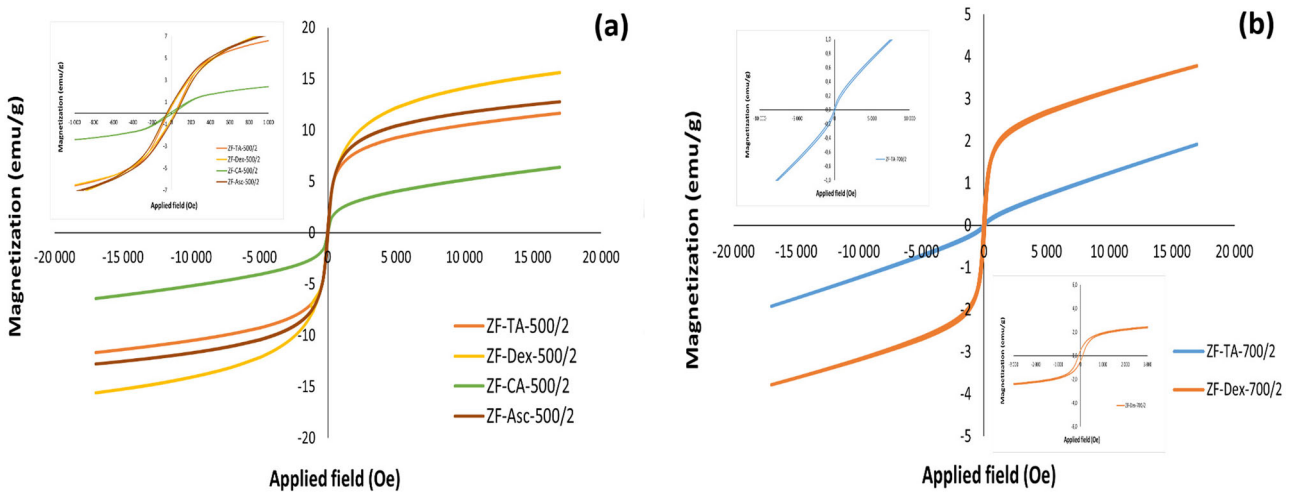

Fig. 4 Results of magnetic properties of zinc ferrite samples calcined at 500 (**a**) or 700 °C (**b**) for 2 h

Table 3 Results of magnetic properties measurements for a series of zinc ferrite samples

Sample name	Coercivity H_C, Oe	Saturation magnetization M_S, emu/g	Remanent magnetization M_r, emu/g	S
ZF–CA–500/2	16.8	6.39	0.096	0.015
ZF–TA–500/2	32.1	11.68	0.551	0.047
ZF–Asc–500/2	46.9	12.77	0.787	0.062
ZF–Dex–500/2	37.0	15.61	0.596	0.038

organic fuel. For the samples calcined at 500 °C, the highest value of saturation magnetization was 15.61 emu/g (ZF–Dex–500/2), which exceeds M_S of the ZF–CA–500/2 sample by more than 2 times. The magnetic properties of samples ZF–TA–700/2 and ZF–Dex–700/2 were also studied, for which the maximum reached magnetization was 1.92 and 3.79 emu/g. Noteworthy, the enhancement in the magnetic properties of zinc ferrite is observed varying the fuel, when tartaric acid is replaced by glucose monohydrate.

The values of coercivity range from 16.8 to 46.9 Oe at the calcination temperature of 500 °C, from 78.1 to 91.9 Oe at 700 °C. Furthermore, for the samples obtained with tartaric acid and glucose monohydrate, an increase in this parameter with rising temperature can be noted. The same trend indicates a higher degree of disorder in the arrangement of magnetic moments at higher calcination temperature [48].

In this work, S varies from 0.014 to 0.121, i.e., does not exceed 0.5 for the studied samples. It is reported in the literature that at $S < 0.5$ the formation of multi-domain structure is observed, while the squareness ratio of at least 0.5 is common for single-domain structures. Low values of this parameter ($S < 0.5$) tend to be associated with multi-domain structures, in which the domain wall motion makes it easier to alter the orientation of the applied field [25, 45, 49].

The magnetic properties of nanomaterials depend on cation distribution, particle size, synthesis method, and chemical composition [50, 51]. The first two factors allow one to interpret the differences in the magnetic properties of $ZnFe_2O_4$ synthesized using different precursors (fuels). A comparative analysis of the studies on zinc ferrite magnetic properties carried out by other authors is provided in Table 4.

Nanomaterials synthesized using the sol-gel method with various organic fuels exhibit primarily moderate ferrimagnetic and paramagnetic properties. The magnetic properties of zinc ferrite presented in [34] should also be taken into account. The saturation magnetization of the synthesized samples exceeds the M_S for ZF–CA–500/2 by 1.7–3.8 times. Properties of nanomaterials are significantly influenced not only by the fuel type but also by heat treatment conditions. By selecting the optimal calcination temperature and heating time, nanomaterials without impurities with high crystallinity and superior magnetic properties to other spinel ferrites can be achieved. Using glycine in [52], a paramagnetic material with moderate saturation magnetization and negligible coercivity was obtained, inferior in these properties to ZF–CA–500/2 and other samples that were studied in this work. The replacement of glycine with another amino acid, arginine, also does not contribute to an increase in the magnetic properties of $ZnFe_2O_4$. The M_S value according to the results of measurements [53] carried

Table 4 The comparison of $ZnFe_2O_4$ magnetic properties

N	Methods	Fuel	Thermal treatment conditions	M_S, emu/g	M_r, emu/g	H_C, Oe	Reference
1	Sol-gel	Ethylenglycol	600 °C, 24 h	8.20	–	0	[28]
2	Sol-gel	Citric acid	350 °C	10.87	0.93	67.3	[34]
3	Sol-gel	Citric acid	450 °C	22.51	2.52	74.8	[34]
4	Sol-gel	Citric acid	550 °C	24.46	2.34	61.6	[34]
5	Microwave combustion	Urea	800 °C, 16 h	1.745	$3.032 \cdot 10^{-3}$	10.11	[12]
6	Sol-gel	Lactose	800 °C, 2 h	0.90	–	–	[54]
7	Microwave combustion	L-Arginine	550 °C, 2.5 h	0.213	0.0515	94.893	[53]
8	Sol-gel auto-combustion	Glycine	800 °C, 5 h	6.02	0.018	21.519	[52]
9	Sol-gel	Tartaric acid, PVA (binder)	200 °C, 2 h	9.02	0.67	47.75	[55]
10	Sol-gel	Tartaric acid, PVA (binder)	400 °C, 2 h	6.95	0.65	75.50	[55]
11	Sol-gel	Tartaric acid, PVA (binder)	600 °C, 2 h	3.85	0.18	68.92	[55]
12	Sol-gel	Tartaric acid, PVA (binder)	800 °C, 2 h	0.04	$2.62 \cdot 10^{-5}$	9.76	[55]
13	Sol-gel	Tartaric acid, PVA (binder)	1000 °C, 2 h	0.03	$1.46 \cdot 10^{-5}$	6.26	[55]
14	Auto-combustion	Sucrose	-	3.70	0.70	84.00	[56]

out with a vibrating magnetometer is not 1 emu/g. This is much lower than the M_S for the synthesized materials.

The use of urea as a fuel allows for the synthesis of zinc ferrite with weak magnetic properties that are comparable to those of ZF–TA–700/2. When disaccharides (lactose and sucrose) are used as fuels, the M_S values are 0.9 and 3.7 emu/g, respectively, which are less than the M_S for ZF–Dex–500/2 and ZF–Dex–700/2.

Therefore, the sol-gel method is a simple way to obtain magnetic materials, whose properties can be optimized by not only altering the composition of the materials, but also by selecting the organic fuel and the calcination temperature.

4 Conclusions

Magnetic zinc ferrite nanomaterials were fabricated by sol-gel method using four organic fuels (citric, tartaric and ascorbic acids and glucose monohydrate) at calcination temperatures of 500 and 700 °C. The formation of $ZnFe_2O_4$ with cubic structure was confirmed for all investigated samples by XRD. The size of zinc ferrite nanocrystallites is 11–39 nm in accordance with the used initial substances and the calcination temperature. The smallest particle size is observed for materials calcined at 500 °C. The magnetic properties of $ZnFe_2O_4$ obtained by sol-gel method using inorganic salts of iron and zinc and ascorbic acid as a fuel were investigated for the first time applying a vibrating magnetometer. Based on the measured magnetic properties, the obtained $ZnFe_2O_4$ is a ferrimagnetic material with adjustable saturation magnetization that depends on the synthesis conditions. The single-phase $ZnFe_2O_4$ materials with small crystallite size and weak manifested magnetic properties were obtained using citric acid as a fuel. At the same time, replacing the fuel with tartaric acid, glucose or ascorbic acid resulted in a significant increase in the saturation magnetization. The results obtained suggest the possibility of using tartaric acid, ascorbic acid and glucose monohydrate as potential fuels for the production $ZnFe_2O_4$ nanomaterials with improved magnetic properties.

Acknowledgements The publication was supported by the Southern Federal University.

Author contributions BE – Writing - Review & Editing, Conceptualization. MM – Investigation, Writing - Original Draft, Visualization. RY – Magnetic properties measurements, Resources. TM – TGA and DSC measurements. All authors reviewed the manuscript.

Compliance with ethical standards

Conflict of interest The authors declare no competing interests.

References

1. Amiri M, Salavati-Niasari M, Akbari A (2019) Magnetic nanocarriers: evolution of spinel ferrites for medical applications. Adv Coll Interface Sci 265:29–44. https://doi.org/10.1016/j.cis.2019.01.003
2. Hojjati-Najafabadi A, Mansoorianfar M, Liang T, Shahin K, Karimi-Maleh H (2022) A review on magnetic sensors for monitoring of hazardous pollutants in water resources. Sci Total Environ 824:153844. https://doi.org/10.1016/j.scitotenv.2022.153844
3. Flores-Rojas GG, López-Saucedo F, Vera-Graziano R, Mendizabal E, Bucio E (2022) Magnetic nanoparticles for medical applications: Updated review. Macromol 2:374–390. https://doi.org/10.3390/macromol2030024
4. Kefeni KK, Msagati TAM, Nkambule TTTTI, Mamba BB (2020) Spinel ferrite nanoparticles and nanocomposites for biomedical

applications and their toxicity. Mater Sci Eng C 107:110314. https://doi.org/10.1016/j.msec.2019.110314
5. Ismael M (2021) Ferrites as solar photocatalytic materials and their activities in solar energy conversion and environmental protection: a review. Sol Energy Mater Sol Cells 219:110786. https://doi.org/10.1016/j.solmat.2020.110786
6. Bohra M, Alman V, Arras R (2021) Nanostructured $ZnFe_2O_4$: an exotic energy material. Nanomaterials 11:1286. https://doi.org/10.3390/nano11051286
7. Garg J, Chiu MN, Krishnan S, Kumar R, Rifah M, Ahlawat P, Jha NK, Kesari KK, Ruokolainen J, Gupta PK (2023) Emerging Trends in Zinc Ferrite Nanoparticles for Biomedical and Environmental Applications. Appl Biochem Biotechnol, https://doi.org/10.1007/s12010-023-04570-2
8. Salih SJ, Mahmood WM (2023) Review on magnetic spinel ferrite (MFe_2O_4) nanoparticles: From synthesis to application. Heliyon 9:e16601. https://doi.org/10.1016/j.heliyon.2023.e16601
9. Tajik S, Safaei M, Beitollahi H (2019) A sensitive voltammetric sertraline nanosensor based on $ZnFe_2O_4$ nanoparticles modified screen printed electrode. Measurement 143:51–57. https://doi.org/10.1016/j.measurement.2019.04.057
10. Hazarika R, Garg A, Chetia S, Phukan P, Kulshrestha A, Kumar A, Bordoloi A, Kalita AJ, Guha AK, Sarma D (2021) Magnetically separable $ZnFe_2O_4$ nanoparticles: A low cost and sustainable catalyst for propargyl amine and NH-triazole synthesis. Appl Catal A Gen 625:118338. https://doi.org/10.1016/j.apcata.2021.118338
11. Nizam T, Thomas M, George M, Joseph A (2022) Adsorption efficiency of sol–gel derived nano metal ferrites, MFe_2O_4 (M = Ni, Zn, Cu) on the removal of Cr (VI) ions from aqueous solution. J Sol Gel Sci Technol 101:618–629. https://doi.org/10.1007/s10971-022-05736-w
12. Al Yaqoob K, Bououdina M, Akhter MS, Al Najar B, Vijaya JJ (2019) Selectivity and efficient Pb and Cd ions removal by magnetic MFe_2O_4 (M = Co, Ni, Cu and Zn) nanoparticles. Mater Chem Phys 232:254–264. https://doi.org/10.1016/j.matchemphys.2019.04.077
13. Manohar A, Krishnamoorthi C, Naidu KCB, Pavithra C (2019) Dielectric, magnetic hyperthermia, and photocatalytic properties of $ZnFe_2O_4$ nanoparticles synthesized by solvothermal reflux method. Appl Phys A 125:477. https://doi.org/10.1007/s00339-019-2760-0
14. Khirade PP, Chavan AR, Somvanshi SB, Kounsalye JS, Jadhav KM (2020) Tuning of physical properties of multifunctional Mg-Zn spinel ferrite nanocrystals: a comparative investigation manufactured via conventional ceramic versus green approach sol-gel combustion route. Mater Res Expr 7:116102. https://doi.org/10.1088/2053-1591/abca6c
15. Suresh R, Rajendran S, Kumar PS, Vo DVN, Cornejo-Ponce L (2021) Recent advancements of spinel ferrite based binary nanocomposite photocatalysts in wastewater treatment. Chemosphere 274:129734. https://doi.org/10.1016/j.chemosphere.2021.129734
16. Kondrashkova IS, Martinson KD, Popkov VI (2023) The effect of Ho-doping on the synthesis, structure and magnetic characteristics of $ZnFe_2O_4$-based nanopowders. J Magn Magn Mater 582:170970. https://doi.org/10.1016/j.jmmm.2023.170970
17. Vidya YS, Manjunatha HC, Sridhar KN, Seenappa L, Munirathnam R, Chinnappareddy B (2023) Brief review on magnetic properties of nanoferrites. Inorg Chem Commun 158:111408. https://doi.org/10.1016/j.inoche.2023.111408
18. Hajalilou A, Mazlan SA (2016) A review on preparation techniques for synthesis of nanocrystalline soft magnetic ferrites and investigation on the effects of microstructure features on magnetic properties. Appl Phys A 122:680. https://doi.org/10.1007/s00339-016-0217-2
19. Vinosha PA, Mely LA, Jeronsia JE, Krishnan S, Das SJ (2017) Synthesis and properties of spinel $ZnFe_2O_4$ nanoparticles by facile co-precipitation route. Optik 134:99–108. https://doi.org/10.1016/j.ijleo.2017.01.018
20. Dippong T, Levei EA, Cadar O (2022) Investigation of structural, morphological and magnetic properties of MFe_2O_4 (M = Co, Ni, Zn, Cu, Mn) obtained by thermal decomposition. Int J Mol Sci 23:8483. https://doi.org/10.3390/ijms23158483
21. Zhu X, Cao C, Su S, Xia A, Zhang H, Li H, Liu Z, Jin C (2021) A comparative study of spinel $ZnFe_2O_4$ ferrites obtained via a hydrothermal and a ceramic route: structural and magnetic properties. Ceram Int, https://doi.org/10.1016/j.ceramint.2021.02.077
22. Kanagesan S, Hashim M, AB Aziz S, Ismail I, Tamilselvan S, Alitheen NB, Swamy MK, Purna Chandra Rao B (2016) Evaluation of antioxidant and cytotoxicity activities of copper ferrite ($CuFe_2O_4$) and zinc ferrite ($ZnFe_2O_4$) nanoparticles synthesized by sol-gel self-combustion method. Appl Sci 6:184. https://doi.org/10.3390/app6090184
23. Hedayati K (2015) Synthesis and characterization of nickel zinc ferrite nanoparticles. J Nanostructures, https://doi.org/10.7508/JNS.2015.01.002
24. Jadhav SA, Khedkar MV, Andhare DD, Gopale SB, Jadhav KM (2021) Visible light photocatalytic activity of magnetically diluted Ni–Zn spinel ferrite for active degradation of rhodamine B. Ceram Int 47:13980–13993. https://doi.org/10.1016/j.ceramint.2021.01.267
25. Dabagh S, Haris SA, Ertas YN (2023) Synthesis, Characterization and Potent Antibacterial Activity of Metal-Substituted Spinel Ferrite Nanoparticles. J Clust Sci 34:2067–2078. https://doi.org/10.1007/s10876-022-02373-9
26. Kumar D, Kumar A, Prakash R, Singh AK (2019) X-ray diffraction analysis of Cu^{2+} doped $Zn_{1-x}Cu_xFe_2O_4$ spinel perovskite phosphors using Williamson-Hall plot method. AIP Conf Proc, https://doi.org/10.1063/1.5122410
27. Yadav RS, Havlica J, Masilko J, Tkacz J, Kuˇritka I, Vilcakova J (2016) Anneal-tuned structural, dielectric and electrical properties of $ZnFe_2O_4$ nanoparticles synthesized by starch-assisted sol–gel auto-combustion method. J Mater Sci Mater Electron 27:5992–6002. https://doi.org/10.1007/s10854-016-4522-5
28. Cobos MA, de la Presa P, Llorente I, García-Escorial A, Hernando A, Jim´enez JA (2020) Effect of preparation methods on magnetic properties of stoichiometric zinc ferrite. J Alloy Compd 849:156353. https://doi.org/10.1016/j.jallcom.2020.156353
29. Bessy TC, Bindhu MR, Johnson J, Chen SM, Chen TW, Almaary KS (2022) UV light assisted photocatalytic degradation of textile waste water by $Mg_{0.8-x}Zn_xFe_2O_4$ synthesized by combustion method and in-vitro antimicrobial activities. Environ Res 204:111917. https://doi.org/10.1016/j.envres.2021.111917
30. Slatineanu T, Diana E, Nica V, Oancea V, Caltun O, Iordan A, Palamaru M (2012) The influence of the chelating/combustion agents on the structure and magnetic properties of zinc ferrite. Open Chem 10:1799–1807. https://doi.org/10.2478/s11532-012-0098-y
31. Hedayati K, Tamiji M, Ghanbari D (2020) Photo-catalyst zinc ferrite-zinc oxide nanocomposites applicable for water purification under solar irradiation. J Sol Energy Res, https://doi.org/10.22059/jser.2020.305457.1161
32. Shanmugavani A, Kalai Selvan R, Layek S, Sanjeeviraja C (2014) Size dependent electrical and magnetic properties of $ZnFe_2O_4$ nanoparticles synthesized by the combustion method: comparison between aspartic acid and glycine as fuels. J Magn Magn Mater 354:363–371. https://doi.org/10.1016/j.jmmm.2013.11.018
33. Sripriya RC, Vigneaswari B, Raj VA (2019) Comparative Studies of Magneto-Optical and Photocatalytic Properties of Magnetically Recyclable Spinel $ZnFe_2O_4$ Nanostructures by Combustion Methods. Int J Nanosci 18:1850020. https://doi.org/10.1142/S0219581X18500205
34. Kannolli A, Avinash P, Manohara SR, Taj M, Kotresh MG (2023) In-depth study of zinc nanoferrite particles at different calcination

temperatures and their behavior in the presence of electric and magnetic fields. J Magn Magn Mater 584:171079. https://doi.org/10.1016/j.jmmm.2023.171079
35. Al Sdran N, Shkir M, Ali HE (2024) Facile combustion-synthesis, structural, morphological, vibrational, photoluminescence, dielectric, and electrical properties of $ZnFe_2O_4$ nanostructures: an effect of citric acid concentration J Alloys Compd, https://doi.org/10.1016/j.jallcom.2024.174540
36. Yao C, Zeng Q, Goya GF, Torres T, Liu J, Wu H, Ge M, Zeng Y, Jiang JZ (2007) $ZnFe_2O_4$ nanocrystals: synthesis and magnetic properties. J Phys Chem C 111:12274–12278. https://doi.org/10.1021/jp0732763
37. Abbasi L, Hedayati K, Ghanbari D (2021) Magnetic properties and kinetic roughening study of prepared polyaniline: lead ferrite, cobalt ferrite and nickel ferrite nanocomposites electrodeposited thin films. J Mater Sci, https://doi.org/10.1007/s10854-021-06006-1
38. Kumar ER, Jayaprakash R, Seehra MS, Prakash T, Kumar S (2013) Effect of α-Fe_2O_3 phase on structural, magnetic and dielectric properties of Mn–Zn ferrite nanoparticles. J Phys Chem Solid, https://doi.org/10.1016/j.jpcs.2013.02.013
39. Dippong T, Levei EA, Cadar O (2021) Formation, structure and magnetic properties of MFe_2O_4@ SiO_2 (M= Co, Mn, Zn, Ni, Cu) nanocomposites. Materials 14:1139. https://doi.org/10.3390/ma14051139
40. Al-Najar B, Younis A, Hazeem L, Sehar S, Rashdan S, Shaikh MN, Albuflasa H, Hankins NP (2022) Thermally induced oxygen related defects in eco-friendly $ZnFe_2O_4$ nanoparticles for enhanced wastewater treatment efficiencies. Chemosphere 288:132525. https://doi.org/10.1016/j.chemosphere.2021.132525
41. Lur'e YY (1989) Spravochnik po analiticheskoi khimii (Handbook of Analytical Chemistry). Khimiya, Moscow
42. Kontoghiorghes GJ, Kolnagou A, Kontoghiorghe CN, Mourouzidis L, Timoshnikov VA, Polyakov NE (2020) Trying to solve the puzzle of the interaction of ascorbic acid and iron: Redox, chelation and therapeutic implications. Medicines 7:45. https://doi.org/10.3390/medicines7080045
43. Yu L, Sun A (2021) Influence of different complexing agents on structural, morphological, and magnetic properties of Mg–Co ferrites synthesized by sol–gel auto-combustion method. J Mater Sci, https://doi.org/10.1007/s10854-021-05711-1
44. Shyamaldas, Bououdina M, Manoharan C (2020) Dependence of structure/morphology on electrical/magnetic properties of hydrothermally synthesized cobalt ferrite nanoparticles. J Magn Magn Mater 493:165703. https://doi.org/10.1016/j.jmmm.2019.165703
45. Kumari N, Kumar V, Khasa S, Singh SK (2015) Chemical synthesis and magnetic investigations on Cr^{3+} substituted Zn-ferrite superparamagnetic nano-particles. Ceram Int 41:1907–1911. https://doi.org/10.1016/j.ceramint.2014.09.118
46. Sapna, Budhiraja N, Kumar V, Singh SK (2018) Tailoring the Structural, Optical and Magnetic Properties of $NiFe_2O_4$ by Varying Annealing Temperature. J Supercond Nov Magn 31:2647–2654. https://doi.org/10.1007/s10948-017-4529-z
47. Al-Abidy M, Al-Nayili A (2023) Enhancement of photocatalytic activities of $ZnFe_2O_4$ composite by incorporating halloysite nanotubes for effective elimination of aqueous organic pollutants. Environ Monit Assess 195:190. https://doi.org/10.1007/s10661-022-10811-4
48. Ge YC, Wang ZL, Yi MZ, Ran LP (2019) Fabrication and magnetic transformation from paramagnetic to ferrimagnetic of $ZnFe_2O_4$ hollow spheres. Trans Nonferrous Met Soc China 29:1503–1509. https://doi.org/10.1016/S1003-6326(19)65057-0
49. Almessiere MA, Slimani Y, Guner S, Nawaz M, Baykal A, Alkhamis F, Sadaqat A, Ercan I (2019) Effect of Nb substitution on magneto-optical properties of $Co_{0.5}Mn_{0.5}Fe_2O_4$ nanoparticles. J Mol Struct 1195:269–279. https://doi.org/10.1016/j.molstruc.2019.05.075
50. Nitika, Rana A, Kumar V (2021) Investigation on anneal-tuned properties of $ZnFe_2O_4$ nanoparticles for use in humidity sensors. Appl Phys A 127:609. https://doi.org/10.1007/s00339-021-04755-8
51. Sapna, Budhiraja N, Kumar V, Singh SK (2019) Shape-controlled synthesis of superparamagnetic $ZnFe_2O_4$ hierarchical structures and their comparative structural, optical and magnetic properties. Ceram Int 45:1067–1076. https://doi.org/10.1016/j.ceramint.2018.09.286
52. Patil K, Jangam K, Patange S, Balgude S, Al-Sehemi AG, Pawar H, More P (2022) Influence of Cu–Mg substituted $ZnFe_2O_4$ ferrite as a highly efficient nanocatalyst for dye degradation and 4-nitrophenol reduction. J Phys Chem Solid 167:110783. https://doi.org/10.1016/j.jpcs.2022.110783
53. Sundararajan M, Sukumar M, Dash CS, Sutha A, Suresh S, Ubaidullah M, Al-Enizi AM, Raza MK, Kumar D (2022) A comparative study on $NiFe_2O_4$ and $ZnFe_2O_4$ spinel nanoparticles: Structural, surface chemistry, optical, morphology and magnetic studies. Phys B Condens Matter 644:414232. https://doi.org/10.1016/j.physb.2022.414232
54. Biglari N, Nasiri A, Pakdel S, Nasiri M (2016) Facile and reliable route for synthesis of zinc ferrite nanoparticles and its application in photo-degradation of methyl orange. J Mater Sci, https://doi.org/10.1007/s10854-016-5456-7
55. Islam S, Rahman ML, Moni MR, Biswas B, Ahmed MF, Sharmin N (2023) Impacts of annealing temperature on microstructure, optical and electromagnetic properties of zinc ferrites nanoparticles synthesized by polymer assisted sol-gel method. Arab J Chem 16:105186. https://doi.org/10.1016/j.arabjc.2023.105186
56. Gabal MA, Al-Mutairi E, Al Angari YM, Awad A, Al-Juaid AA, Saeed A (2022) Synthesis, characterization, elastic, and electromagnetic properties of MFe_2O_4 ferrites (M= Co^{2+}, Ni^{2+}, Cu^{2+}, Mg^{2+}, and Zn^{2+}) via sucrose auto-combustion. J Mater Res 37:2257–2270. https://doi.org/10.1557/s43578-022-00624-z
57. Levy D, Pavese A, Hanfland M (2000) Phase transition of synthetic zinc ferrite spinel ($ZnFe_2O_4$) at high pressure, from synchrotron X-ray powder diffraction. Phys Chem Miner 27:638–644. https://doi.org/10.1007/s002690000117

Publisher's note Springer Nature remains neutral with regard to jurisdictional claims in published maps and institutional affiliations.

Springer Nature or its licensor (e.g. a society or other partner) holds exclusive rights to this article under a publishing agreement with the author(s) or other rightsholder(s); author self-archiving of the accepted manuscript version of this article is solely governed by the terms of such publishing agreement and applicable law.